A direct link between *Prss53*, hair curvature, and skeletal dysplasia

Jichao Deng[1], Yuning Song[1], Hongmei Liu[1], Tingting Sui[1], Mao Chen[1], Yuxin Zhang[1], Bing Yao[1], Yuxin Xu[1], Zhiquan Liu[1], Liangxue Lai[1,2]*, Zhanjun Li[1]*

1 Key Laboratory of Zoonosis Research, Ministry of Education, Jilin University, Changchun 130062, China

2 Guangzhou Regenerative Medicine and Health Guangdong Laboratory, 510005 Guangzhou, China

* To whom correspondence should be addressed:

Tel: (86)431-87836176; Fax: (86)431-87980131;

E-mail: lizj_1998@jlu.edu.cn (Zhanjun Li); lai_liangxue@gibh.ac.cn (Liangxue Lai);

Abstract

In humans, protease serine S1 family member 53 (Prss53) is highly expressed in the hair follicle, especially the inner root sheath, which is associated with hair shape according to recent genome-wide association study (GWAS) data. However, no animal evidence has indicated a link between *Prss53* and hair shape to date . Here, we used CRISPR/Cas9 to generate *Prss53*-mutated rabbits. The homozygous (*Prss53*$^{-/-}$) rabbits exhibited curved hair and skeletal dyskinesia with severe malformation , while the heterozygous (*Prss53*$^{+/-}$) rabbits did not exhibit these features. The curvature features of the hair were accompanied by lesions that were generally denser and less well-defined in the cuticular septation of the hair shaft, and the compartments of the hair follicle were incomplete, as evidenced by decreased expression levels of keratinocyte differentiation genes. In addition, skeletal dysplasia, an increased lethality rate and decreased plasma calcium and serum alkaline phosphatase (ALP) levels were determined in the *Prss53*$^{-/-}$ rabbits. Furthermore, disrupted calcium metabolism, which may play a role in the hair curvature and skeletal dysplasia of *Prss53*$^{+/-}$ rabbits, was demonstrated by using high-throughput RNA sequencing data. Thus, our study confirmed for the first time that the loss of *Prss53* lead to curved hair in animals and provides new insights into the crucial role of *Prss53* in calcium metabolism.

Author Summary:

No animal evidence has indicated a link between *Prss53* and hair shape to date.

The *Prss53*$^{-/-}$ rabbits exhibited curved hair and skeletal dyskinesia.

The disrupted calcium metabolism may play a role in the hair curvature and skeletal dysplasia of *Prss53*$^{+/-}$ rabbits.

Keywords: Prss53, hair curvature, keratinocyte differentiation, calcium metabolism, skeletal dysplasia

Introduction

Membrane-anchored serine proteases regulate fundamental cellular and developmental processes, including orchestrating neural tube closure, erecting barriers between cells, developing the inner ear, regulating apical sodium entry and fluid volume, controlling the natriuretic peptide system, adjusting cellular iron export to satisfy iron needs, and promoting fertilization[1]. PRSS53, a member of the membrane-anchored serine proteases, hydrolyzes peptide bonds[2] and is highly expressed in the hair follicle IRS, medulla, precortex and some melanocytes[3].

Previous studies reported that *Prss53* is a psoriasis susceptibility locus and is linked to systemic lupus erythematosus, suggesting its potential roles in skin function[4-7]. The Q30R SNP in *Prss53* may influence hair shape and is involved in the human variation of head hair shape among different continental groups[3,8]. In addition, ENaC activity is regulated by the activity of a channel-activating protease of Prss8 (a homologous gene of *Prss53*), implying the *Prss53* may have an indispensable role in ion channel activity[9].

The triggering of hair curvature is clearly related to symmetry or asymmetry axis formation in follicles and includes Wnt, TGFβ, BMP, Shh and FGFs, etc. [10,11]. In particular, the Wnt/Ca^{2+} and Wnt/planar cell polarity (PCP) pathways are additional novel mechanisms that affect hair shape[12]. Furthermore, disruptions in calcium

metabolism may contribute to a wide variety of clinical symptoms, including osteoporosis, osteolysis, nephrocalcinosis and adynamie[13].

Here, we successfully generated *Prss53*-deficient rabbits. These rabbits exhibited curved hair, severe skeletal malformation and disrupted calcium metabolism. Altogether, these data suggest that *Prss53* may play an important role in calcium metabolism and provide the first direct evidence that *Prss53* functions in hair curvature shape and skeletal dysplasia.

Results

Prss53 expression pattern

To explore the function of the *Prss53* gene, the expression pattern was determined, as shown in Figure 1. The EST profile data suggest extensive expression of *Prss53* in the skin and bone in Homo sapiens . In addition, high *Prss53* expression in the developing inner root sheath (IRS), precortex and medulla of the hair follicle has been reported in a previous study[3], but the *Prss53* expression pattern in bone has not been determined.

Generation of *Prss53*$^{-/-}$ rabbits via the CRISPR/Cas9 system

Prss53, a candidate gene for curly hair, was found in a recent GWAS in Latin Americans of mixed European and Native American origin[3]. To disrupt the function of rabbit *Prss53,* two sgRNAs targeting the third and fourth exon of *Prss*53 were designed (Figure 2A) and transferred to embryos. Then, the genomic DNA from each pup was isolated, and *Prss53* gene mutations were detected via PCR and Sanger sequencing. As shown in Figure S1B, F0 rabbits carrying *Prss53* mutations were obtained and were used for the following study. An off-target assay showed that the CRISPR/Cas9 system did not induce undesirable off-target effects in the *Prss53* knockout (KO) rabbits (Supplementary Material, Figure. S2).

To obtain a sufficient number of rabbits for a detailed functional study of *Prss53*, the sexually mature F0 founder was mated with wildtype (WT) female rabbits, and then the heterozygous (*Prss53*$^{+/-}$) rabbits were mated and used to generate homozygous (*Prss53*$^{-/-}$) rabbits (Figure. S3). These results demonstrated that

mutations in *Prss53* can be achieved via the CRISPR/Cas9 system with high efficiency in rabbits.

Hair curvature and skeletal dysplasia in *Prss53*$^{-/-}$ rabbits

Prss53 encodes a polyserine protease called polyserase-3 (POL3S) and is expressed in the IRS, medulla, and precortex of hair follicles and in melanocytes[3]. In our study, curved hair curvature was present all over the body of *Prss53*$^{-/-}$ rabbits (Figure. 2B and S1A). The hair length was not different among the rabbits, but the *Prss53*$^{-/-}$ rabbits had significantly finer hair than that of the WT rabbits (Figure. 2C and D). In addition, impaired physical activity was determined in the *Prss53*$^{-/-}$ rabbits, with a larger knee range of motion compared to the WT rabbits (Figure. 2E and F). The *Prss53*$^{-/-}$ rabbits exhibited a significantly increased lethality rate during postnatal week 6 (~12.5% survive to adulthood) (Figure. 2G).

To further study whether the protein level of *Prss53* was disrupted in the *Prss53*$^{-/-}$ rabbits, we performed a 3D model protein structure prediction, Western blotting and immunofluorescence staining. The results indicated a disrupted protein structure (Figure. 3A and B). The complete loss of PRSS53 protein (Figure. 3C and D) was determined in the *Prss53*$^{-/-}$ rabbits when compared with the WT rabbits. Furthermore, the immunohistochemical results confirmed the complete loss of PRSS53 protein in the hair follicles (Figure. 3E and F) and bone marrow (Figure. 3G and H) of the *Prss53*$^{-/-}$ rabbits. These results confirmed that *Prss53* plays an important role in maintaining hair shape and skeletal health.

Abnormal keratinocyte differentiation in *Prss53*$^{-/-}$ rabbits

A previous study reported that abnormal keratinocyte differentiation negatively affects the hair shaft extension and hair shaft shape[14]. In this study, H&E staining showed no significant pathological changes of the hair follicles in the *Prss53*$^{-/-}$ rabbits (Figure. 4A). Next, we examined the hair structure by scanning electron microscopy (SEM). As illustrated in Figure. 4C, the medullated fibers and unmyelinated hair from WT rabbits exhibited well-defined and regular cuticular septation, while the *Prss53*$^{-/-}$

rabbits presented lesions and less well-defined cuticular septation. Furthermore, transmission electron microscopy (TEM) analyses were performed on the skin from the dorsum of *Prss53*$^{-/-}$ and WT rabbits. The results showed that the WT rabbits exhibited a clear structure, including IRS and cuticle, while the *Prss53*$^{-/-}$ rabbits fail to develop the cuticle (Figure. 4D). High-throughput sequencing revealed significantly decreased expression of keratinocyte differentiation genes, including *Lats1, Yap1, Adam9, Csta, Krt10, Wnt16 and Tp63,* in the *Prss53*$^{-/-}$ rabbits compared with the WT rabbits (Figure. 4B). The results showed abnormal keratinocyte differentiation in the *Prss53*$^{-/-}$ rabbits.

Disrupted calcium metabolism in *Prss53*$^{-/-}$ rabbits

Extracellular calcium and 1,25$(OH)_2$D raise intracellular free calcium as a necessary step toward stimulating keratinocyte differentiation[15]. To uncover whether *Prss53* influences hair shape by regulating calcium metabolism, high-throughput RNA sequencing was used to compare the gene expression patterns between the *Prss53*$^{-/-}$ and WT rabbits. As shown in Figure. 5A, good internal controls and high correlations were determined in the *Prss53*$^{-/-}$ and WT rabbits. The up-regulated and down-regulated genes are shown in Figure. 5B. Furthermore, Gene Ontology (GO) and Kyoto Encyclopedia of Genes and Genomes (KEGG) analyses revealed significantly upregulated calcium ion binding genes and the calcium signaling pathway in the *Prss53*$^{-/-}$ rabbits compared with the WT rabbits (Figure. 5C and Table 1). Thus, we suspected that abnormal calcium metabolism is responsible for the hair curvature phenotype of the *Prss53*$^{-/-}$ rabbits (Figure. 5D).

Disrupted osteoblast differentiation in *Prss53*$^{-/-}$ rabbits

Disordered calcium metabolism may induce osteoporosis and osteolysis in clinical settings[13]. To further examine whether disrupted calcium metabolism is responsible for the skeletal dysplasia, the skeletal and a serum biochemical analysis were compared between the *Prss53*$^{-/-}$ and WT rabbits. As shown in Figure. 6A, the *Prss53*$^{-/-}$ rabbits exhibited more severe knee abnormalities and were substantially

more malformed than WT rabbits by X-ray autoradiograph examination. The serum biochemical analysis demonstrated significantly decreased plasma calcium and ALP levels in the *Prss53*$^{-/-}$ rabbits (Figure. 6B and C). In addition, immunohistochemistry and H&E staining confirmed the significantly reduced number of osteoblasts and the complete loss of PRSS53 protein in the *Prss53*$^{-/-}$ rabbits (Figure. 6D, E and F) compared to the WT control. Hence, disrupted calcium metabolism is responsible for the skeletal abnormalities in the *Prss53*$^{-/-}$ rabbits.

In summary, our study provides the first evidence that *Prss53* plays an important role in calcium metabolism, which is responsible for keratinocyte and osteoblast differentiation and, thereby, maintains the normal morphology of the hair and skeleton (Figure. 5D).

Discussion

To date, the function *Prss53* was largely unknown, and limited information regarding *Prss53* mutant animals was available. In this study, we first generated a stably transmitted *Prss53* mutant rabbit via the CRISPR/Cas9 system. Interestingly, the hair curvature phenotype of the *Prss53*$^{-/-}$ rabbits is consistent with the Latin American population of mixed European and Native American origin with a Q30R substitution in *Prss53* [3].

Uncombable hair syndrome is characterized by dry, frizzy, and spangly hair, which has longitudinal grooves and a heart-shaped cross section by SEM[16]. Consistently, lesions and less well-defined cuticular septation were determined in the *Prss53*$^{-/-}$ rabbits in our study. In addition, high-throughput RNA sequencing data revealed significantly decreased expression of keratinocyte differentiation genes, including *Lats1*[17], *Yap1*[18], *Adam9*[19], *Csta*[20], *Krt10*[21], *Wnt16*[22]and *Tp63*[23], in *Prss53*$^{-/-}$ rabbits compared with WT rabbits, A previous study showed that the hair shaft is derived from the progeny of keratinocyte stem cells in the follicular epithelium, and the growth and differentiation of follicular keratinocytes is guided by a specialized mesenchymal population[14]. Therefore, abnormal keratinocyte differentiation is

responsible for disruptions to hair shaft shape, indicating that *Prss53* may play an important role in maintaining keratinocyte differentiation.

Unexpectedly, impaired physical activity and decreased plasma calcium may be responsible for the early death of *Prss53*$^{-/-}$ rabbits. Calcium is essential for bone development by promoting osteogenesis and inhibiting osteoclast activity through increased osteoprotegerin secretion from osteoblasts[24]. Alkaline phosphatase is widely used as a marker of osteoblast differentiation and was significant decreased in the *Prss53*$^{-/-}$ rabbits when compared with WT rabbits. Previous studies reported that osteoblast differentiation is closely associated with skeletal development, such as in *Med23*-deficient MSCs or preosteoblasts that display defective bone formation and impaired osteoblast differentiation[25]. *Runx2*$^{-/-}$ mice lack both mature osteoblasts and a mineralized skeleton[26,27]. Hence, this study is the first report to demonstrate that disrupted osteoblast differentiation in the *Prss53* mutant is responsible for skeletal abnormalities, suggesting that *Prss53* may have an indispensable role in skeletal development.

In this study, the significantly reduced number of osteoblasts and disrupted calcium metabolism were determined in the *Prss53*$^{-/-}$ rabbits by RNA sequencing technology. The G-protein-coupled receptor (CaR) is not limited to the parathyroid gland [28] , and also inkeratinocytes[29]. The calcium-sensing receptor, transient receptor potential channels, and STIM/Orai also function in calcium sensing and calcium entry in keratinocytes[30]. In addition, both extracellular calcium and 1,25$(OH)_2$D raise the level of intracellular free calcium as a necessary step toward stimulating keratinocyte differentiation[15]. Accumulating studies have shown that calcium oscillations via restraints of major Ca^{2+} entry sources (extracellular Ca^{2+} influx and intracellular Ca^{2+} release from the endoplasmic reticulum) is required for osteoblast differentiation[31]. Hence, we hypothesize that disrupted calcium metabolism is responsible for abnormal keratinocyte differentiation in the *Prss53*$^{-/-}$ rabbits.

To the best of our knowledge, this study is the first animal report on hair curvature and skeletal dysplasia caused by a *Prss53* mutation in rabbits and provides

evidence that *Prss53* is required for keratinocyte and osteoblast differentiation, which is essential for hair and skeletal cell proliferation.

Materials and Methods

1 Ethical statement

New Zealand rabbits were obtained from the Laboratory Animal Center of Jilin University. All rabbit experiments were conducted under the approval of the Animal Care Center and Use Committee of Jilin University.

2 sgRNA design and vector construction

The 3xFLAG-NLS-SpCas9-NLS vector (Addgene ID 48137) was linearized with *NotI* and *in vitro* transcribed using a mMessage mMachine SP6 Kit (Ambion) and RNeasy Mini Kit (Qiagen), according to the manufacturer's instructions.

The design of targeted sgRNAs was described previously (http://crispr.mit.edu/) [32]. Complementary oligo sgRNAs were cloned into the *BbsI* sites of a Puc57-T7-sgRNA cloning vector (Addgene ID 51306). The Puc57-T7-sgRNA vector was amplified by PCR with T7 primers (T7-F: 5'-GAA ATT AAT ACG ACT CAC TAT A-3' and T7-R: 5'-AAA AAA AGC ACC GAC TCG GTG CCA C-3'), and then, the PCR products were *in vitro* transcribed using a MAXIscript T7 Kit (Ambion, USA) and purified with a miRNeasy Mini Kit (Qiagen, Germany), according to the manufacturer's instructions.

3 Microinjection and embryo transfer

The procedures of embryo microinjection and embryo transfer were previously described [33,34]. Briefly, female New Zealand white rabbits (6–8 months old) were superovulated with FSH (50 IU) every 12 h for 3 days. After the last injection, the female rabbits were mated with male rabbits and were then injected with 100 IU of human chorionic gonadotrophin (hCG). Rabbit embryos at the pronuclear stage were collected and transferred into oocyte manipulation medium. A mixture of Cas9 and sgRNA mRNA (200 ng/μl and 40 ng/μl, respectively) was microinjected into the embryo cytoplasm. The injected embryos were transferred to EBSS medium for

short-term culture at 38.5°C, 5% CO_2 and 100% humidity conditions. Approximately 30–50 injected zygotes were transferred into the oviducts of recipient rabbits.

4 Mutation detection in pups by PCR

Genomic DNA from WT and *Prss53* mutant rabbits was isolated using a TIANamp Genomic DNA Kit (TIANGEN, Beijing, China). The DNA was amplified by 2×Taq Plus MasterMix (TIANGEN), and the PCR primers used to detect mutations were as follows: rabbits-F-5' CAG GAA GTT CCA GTC ACT TGT -3', rabbits-R-5' GGT TGA GAA GGA AGG GAG ATT AG-3'. The PCR products were purified and cloned into the pGM-T vector (TIANGEN, Beijing, China); at least 10 positive plasmid clones were sequenced and analyzed using NCBI BLAST.

5 Western blot

Western blot analysis was performed as described previously[35]. Samples from the head skin of *Prss53*$^{-/-}$ and WT rabbits were homogenized and lysed in RIPA buffer supplemented with 2.5 μL/mL protease inhibitor cocktail (Roche) on ice for 30 min. Anti-*Prss53* (1:1000, Novus) were used as primary antibody, and β-actin antibody (1:2000, Abcam) was used as loading control.

6 Histopathology and immunohistochemistry

H&E staining was performed as previously described [33]. Briefly, the tissues were collected from WT and *Prss53*$^{-/-}$ rabbits, fixed in 4% paraformaldehyde for 48 h, embedded in paraffin wax, sectioned for slides, and stained with H&E.

The immunohistochemistry staining was performed as previously described[36]. Primary antibodies against *Prss53* (1:500, Novus) and secondary anti-rabbit polyclonal antibodies (1:1000, Beyotime Institute of Biotechnology, Shanghai, China) were used. The slides were imaged with a Nikon ts100 microscope and processed using Photoshop CS5 (Adobe).

7 Scanning electron microscopy (SEM)

Scanning electron microscopy (SEM) was performed as described previously[37]. The hair from the heads of *Prss53*$^{-/-}$ and WT rabbits was attached onto specimen stubs using double-sided conductive tabs and sputter-coated with gold using a Polaron SEM E-1010. Samples were imaged using a S-3400N Scanning Electron Microscope.

8 Transmission electron microscopy (TEM)

Transmission electron microscopy was performed as described previously[38]. The skin from the dorsum of *Prss53*$^{-/-}$ and WT rabbits was fixed in 3% glutaraldehyde for 4 h at 4°C. Ultrathin longitudinal sections of the skin were cut with an ultramicrotome and a diamond knife and processed for examination by transmission electron microscope (TEM) (H-7640, Hitachi, Japan).

9 Skeletal histomorphology

X-ray autoradiography pictures of the *Prss53*$^{-/-}$ and WT rabbits were taken as previously described [33]. Briefly, the YEMA Radiography System with a digital camera attached (Varian, USA) on X-ray film (ROTANODE, Japan) was used in this study. The images were taken at 40 KV with 3 mA exposure.

10 Statistical analysis

Data were statistically analyzed with GraphPad prism software (t test), and $p < 0.05$ was considered statistically significant. *$p < 0.05$, **$p < 0.01$, ***$p < 0.001$, **** $p < 0.0001$.

Abbreviation： Prss53, serine protease 53; ALP, alkaline phosphatase; POL3S, polyserine protease called polyserase-3; CAP, channel-activating protease; PCP, planar cell polarity; IRS, inner root sheath; KO, knockout; WT, wildtype; HF, hair follicle; SEM, scanning electron microscope; TEM, transmission electron microscopy; GO, gene ontology; KEGG, Kyoto encyclopedia of genes and genomes; CaR, G-protein-coupled receptor.

Acknowledgments

The authors express their gratitude to Peiran Hu at the Embryo Engineering Center for technical assistance.

This study was financially supported by the National Key Research and Development Program of China Stem Cell and Translational Research (2017YFA0105101), the Program for Changjiang Scholars and Innovative Research Team in University (No. IRT_16R32), and Key Research & Development Program of

Guangzhou Regenerative Medicine and Health Guangdong Laboratory (2018GZR110104004).

Author Contributions: J.D., L.L., and Z.L. designed the research. J.D., Y.S., and T.S. performed the research. J.D., H.L., M.C., and B.Y. contributed new reagents or analytic tools. J.D., Y.Z., Y.X., and Z.L. analyzed the data. J.D., Z.L., and L.L. wrote the paper. All authors have read and approved the final manuscript.

Competing financial interests: The authors declare no competing financial interests.

References

1 Szabo, R. & Bugge, T. H. Membrane-Anchored Serine Proteases in Vertebrate Cell and Developmental Biology. *Annual Review of Cell and Developmental Biology, Vol 27* **27**, 213-235, doi:10.1146/annurev-cellbio-092910-154247 (2011).

2 Szpak, M. *et al.* FineMAV: prioritizing candidate genetic variants driving local adaptations in human populations. *Genome Biol* **19**, doi:Artn 5 10.1186/S13059-017-1380-2 (2018).

3 Adhikari, K. *et al.* A genome-wide association scan in admixed Latin Americans identifies loci influencing facial and scalp hair features. *Nature communications* **7**, 10815, doi:10.1038/ncomms10815 (2016).

4 Tsoi, L. C. *et al.* Identification of 15 new psoriasis susceptibility loci highlights the role of innate immunity. *Nature genetics* **44**, 1341-1348, doi:10.1038/ng.2467 (2012).

5 Almlof, J. C. *et al.* Novel risk genes for systemic lupus erythematosus predicted by random forest classification. *Scientific reports* **7**, 6236, doi:10.1038/s41598-017-06516-1 (2017).

6 Budu-Aggrey, A., Bowes, J. & Barton, A. Identifying a novel locus for psoriatic arthritis. *Rheumatology* **55**, 25-32, doi:10.1093/rheumatology/kev273 (2016).

7 Swindell, W. R. *et al.* Modulation of Epidermal Transcription Circuits in Psoriasis: New Links between Inflammation and Hyperproliferation. *Plos One* **8**, doi:ARTN e79253 10.1371/journal.pone.0079253 (2013).

8 Liu, F. *et al.* Meta-analysis of genome-wide association studies identifies 8 novel loci involved in shape variation of human head hair. *Hum Mol Genet* **27**, 559-575, doi:10.1093/hmg/ddx416 (2018).

9 Vallet, V., Chraibi, A., Gaeggeler, H. P., Horisberger, J. D. & Rossier, B. C. An epithelial serine protease activates the amiloride-sensitive sodium channel. *Nature* **389**, 607-610, doi:10.1038/39329 (1997).

10 Vandenberg, L. N. & Levin, M. Perspectives and open problems in the early phases of left-right patterning. *Semin Cell Dev Biol* **20**, 456-463, doi:10.1016/j.semcdb.2008.11.010 (2009).

11 Vandenberg, L. N. & Levin, M. Far from solved: a perspective on what we know about early

mechanisms of left-right asymmetry. *Developmental dynamics : an official publication of the American Association of Anatomists* **239**, 3131-3146, doi:10.1002/dvdy.22450 (2010).

12 Nissimov, J. N. & Das Chaudhuri, A. B. Hair curvature: a natural dialectic and review. *Biological reviews of the Cambridge Philosophical Society* **89**, 723-766, doi:10.1111/brv.12081 (2014).

13 Kasperk, C. & Bartl, H. Disorders of calcium metabolism. *Internist* **55**, 1313-1326, doi:10.1007/s00108-014-3610-y (2014).

14 Chi, W., Wu, E. & Morgan, B. A. Dermal papilla cell number specifies hair size, shape and cycling and its reduction causes follicular decline. *Development* **140**, 1676-1683, doi:10.1242/dev.090662 (2013).

15 Bikle, D. D., Ng, D., Tu, C. L., Oda, Y. & Xie, Z. Calcium- and vitamin D-regulated keratinocyte differentiation. *Molecular and cellular endocrinology* **177**, 161-171 (2001).

16 FB, U. B. *et al.* Mutations in Three Genes Encoding Proteins Involved in Hair Shaft Formation Cause Uncombable Hair Syndrome. *American journal of human genetics* **99**, 1292-1304, doi:10.1016/j.ajhg.2016.10.004 (2016).

17 Nishio, M. *et al.* Cancer susceptibility and embryonic lethality in Mob1a/1b double-mutant mice. *J Clin Invest* **122**, 4505-4518, doi:10.1172/JCI63735 (2012).

18 Sambandam, S. A. T. *et al.* 14-3-3 sigma Regulates Keratinocyte Proliferation and Differentiation by Modulating Yap1 Cellular Localization. *Journal of Investigative Dermatology* **135**, 1621-1628, doi:10.1038/jid.2015.42 (2015).

19 Tanasubsinn, P. *et al.* Overexpression of ADAM9 in oral squamous cell carcinoma. *Oncol Lett* **15**, 495-502, doi:10.3892/ol.2017.7284 (2018).

20 Chen, H. B. *et al.* Understanding Haemophilus parasuis infection in porcine spleen through a transcriptomics approach. *Bmc Genomics* **10**, doi:Artn 64 10.1186/1471-2164-10-64 (2009).

21 Huang, K. F., Ma, K. H., Liu, P. S., Chen, B. W. & Chueh, S. H. Ultraviolet B irradiation increases keratin 1 and keratin 10 expressions in HaCaT keratinocytes via TRPV1 activation and ERK phosphorylation. *Experimental dermatology* **26**, 832-835, doi:10.1111/exd.13292 (2017).

22 Teh, M. T. *et al.* Role for WNT16B in human epidermal keratinocyte proliferation and differentiation (vol 120, pg 330, 2007). *Journal of cell science* **120**, 917-917, doi:Doi 10.1242/Jcs.03421 (2007).

23 Katoh, I. *et al.* Repression of Wnt/beta-catenin response elements by p63 (TP63). *Cell Cycle* **15**, 699-710, doi:10.1080/15384101.2016.1148837 (2016).

24 Cao, C. *et al.* Increased Ca2+signaling through altered CaV1.2 L-type Ca2+channel activity promotes bone formation and prevents estrogen deficiency-induced bone loss. *J Bone Miner Res* **32**, S31-S31 (2017).

25 Liu, Z. *et al.* Mediator MED23 cooperates with RUNX2 to drive osteoblast differentiation and bone development. *Nature communications* **7**, doi:Artn 11149 10.1038/Ncomms11149 (2016).

26 Komori, T. *et al.* Targeted disruption of Cbfa1 results in a complete lack of bone formation owing to maturational arrest of osteoblasts. *Cell* **89**, 755-764 (1997).

27 Mundlos, S. *et al.* Mutations involving the transcription factor CBFA1 cause cleidocranial dysplasia. *Cell* **89**, 773-779 (1997).

28 Garrett, J. E. *et al.* Molecular cloning and functional expression of human parathyroid calcium

receptor cDNAs. *J Biol Chem* **270**, 12919-12925 (1995).

29 Bikle, D. D., Ratnam, A., Mauro, T., Harris, J. & Pillai, S. Changes in calcium responsiveness and handling during keratinocyte differentiation. Potential role of the calcium receptor. *J Clin Invest* **97**, 1085-1093, doi:10.1172/JCI118501 (1996).

30 Elsholz, F., Harteneck, C., Muller, W. & Friedland, K. Calcium - a central regulator of keratinocyte differentiation in health and disease. *Eur J Dermatol* **24**, 650-661, doi:10.1684/ejd.2014.2452 (2014).

31 Li, Z. *et al.* Regulator of G protein signaling protein 12 (Rgs12) controls mouse osteoblast differentiation via calcium channel/oscillation and Galphai-ERK signaling. *J Bone Miner Res*, doi:10.1002/jbmr.3645 (2018).

32 Cong, L. *et al.* Multiplex Genome Engineering Using CRISPR/Cas Systems. *Science* **339**, 819-823, doi:10.1126/science.1231143 (2013).

33 Sui, T. T. *et al.* CRISPR/Cas9-mediated mutation of PHEX in rabbit recapitulates human X-linked hypophosphatemia (XLH). *Hum Mol Genet* **25**, 2661-2671, doi:10.1093/hmg/ddw125 (2016).

34 Amoasii, L. *et al.* Single-cut genome editing restores dystrophin expression in a new mouse model of muscular dystrophy. *Sci Transl Med* **9**, doi:10.1126/scitranslmed.aan8081 (2017).

35 Han, K. *et al.* Generation of Hoxc13 knockout pigs recapitulates human ectodermal dysplasia-9. *Hum Mol Genet* **26**, 184-191, doi:10.1093/hmg/ddw378 (2017).

36 Oros, J., Lopez-Yanez, M., Rodriguez, F., Calabuig, P. & Castro, P. L. Immunohistochemical staining patterns of alpha-keratins in normal tissues from two reptile species: implications for characterization of squamous cell carcinomas. *BMC veterinary research* **14**, 219, doi:10.1186/s12917-018-1545-6 (2018).

37 Combalia, A., Brugues, A., Garcia-Veigas, F. J. & Ferrando, J. Scanning Electron Microscopy and X-ray Microanalysis of Reconstructive Hair Fibers. *International journal of trichology* **9**, 54-57, doi:10.4103/ijt.ijt_100_16 (2017).

38 Sanad, E. M., El-Esawy, F. M., Mustafa, A. I. & Agina, H. A. Structural changes of hair shaft after application of chemical hair straighteners: Clinical and histopathological study. *Journal of cosmetic dermatology*, doi:10.1111/jocd.12752 (2018).

Figure Legends

Figure. 1. *Prss53* expression pattern

Schematic diagram of the extensive expression of *Prss53* in the lung, stomach, brain, eye, and skin. Bone expression was not determined by the UniGene database. The expression of *Prss53* was mainly detected in the developing IRS, precortex and medulla of the hair follicle.

Figure. 2. Hair curvature and skeletal abnormalities in *Prss53*$^{-/-}$ rabbits

(A) Schematic diagram of two sgRNA target sites located in exons 3 and 4 of rabbit *Prss53*. *Prss53* exons are indicated by rectangles; the target sites of the two sgRNA sequences, namely, sgRNA1 and sgRNA2, are highlighted in red; the protospacer-adjacent motif (PAM) sequence is highlighted in green. **(B)** The hair curvature in a F0 *Prss53*$^{-/-}$ rabbit generated by the CRISPR/Cas9 system. **(C)** No significant difference in the hair length was determined in *Prss53*$^{-/-}$ rabbits compared with WT rabbits. **(D)** Statistical analysis showed a decreased hair diameter in the head of *Prss53*$^{-/-}$ rabbits. **(E)** Impaired physical activity was determined in *Prss53*$^{-/-}$ rabbits compared with WT rabbits. **(F)** Statistical analysis showed a decreased range of motion in the ankles of *Prss53*$^{-/-}$ rabbits. **(G)** Survival curves of *Prss53*$^{-/-}$ rabbits compared with WT controls.

Figure. 3. The loss of PRSS53 protein in *Prss53*$^{-/-}$ rabbits

(A and B) Computer modeling of the 3D structure of WT and mutant *Prss53*. **(C and D)** Western blot results showed the complete loss of PRSS53 protein in the skin of *Prss53*$^{-/-}$ rabbits. **(E and F)** Immunohistochemistry staining showed the complete loss of PRSS53 protein in the hair follicles of *Prss53*$^{-/-}$ rabbits. Black arrow indicates the expression of PRSS53 protein in the hair follicles of WT rabbits. **(G and H)** Immunohistochemistry staining showed the complete loss of PRSS53 protein in the proerythroblasts of *Prss53*$^{-/-}$ rabbits. Red arrow indicates the expression of PRSS53 protein in the proerythroblasts of WT rabbits.

Figure. 4. Abnormal keratinocyte differentiation in *Prss53*$^{-/-}$ rabbits

(A) No significant difference in the HF was determined in the *Prss53*$^{-/-}$ rabbits compared with WT rabbits. **(B)** The heat map shows the significantly decreased expression of keratinocyte differentiation genes, including LATS1, YAP1, ADAM9, CSTA, KRT10, WNT16 and TP63, in *Prss53*$^{-/-}$ rabbits compared with WT rabbits **(C)** SEM analysis of WT and *Prss53*$^{-/-}$ hair fibers shows that medullated fibers and unmyelinated hair from WT rabbits exhibit well-defined and regular cuticular septation, while medullated fibers and unmyelinated hair from *Prss53*$^{-/-}$ rabbits reflect lesions that appear generally denser and less well-defined areas in the cuticular septation. **(D)** TEM analysis of WT and *Prss53*$^{-/-}$ skin shows that WT rabbits exhibited a clear structure, while the *Prss53*$^{-/-}$ rabbits fail to develop the cuticle. Red arrow indicates the location of the IRS in hair follicle of WT and *Prss53*$^{-/-}$ rabbits; green arrow indicates the location of the cuticle in the hair follicle of WT rabbits; yellow arrow indicates lesions and less well-defined areas in the cuticular septation.

Figure. 5. Disrupted calcium metabolism in *Prss53*$^{-/-}$ rabbits

(A) Internal consistency, homogeneity and high correlations were determined in the WT and *Prss53*$^{-/-}$ rabbits. **(B)** Volcano plot shows that a large number of differentiated genes (upregulation and downregulation) was detected between WT and *Prss53*$^{-/-}$ rabbits. Blue dots indicate upregulated genes; red dots indicate downregulated genes. **(C)** Heap map showing significantly upregulated calcium metabolism genes in the *Prss53*$^{-/-}$ rabbits compared with WT rabbits. **(D)** Schematic diagram of the role of *Prss53* in calcium metabolism, which is responsible for keratinocyte differentiation and osteoblast differentiation to maintain the normal morphology of the hair and skeleton.

Figure. 6. Disrupted osteoblast differentiation in *Prss53*$^{-/-}$ rabbits

(A) X-ray autoradiography was used to characterize the skeleton in WT and *Prss53*$^{-/-}$ rabbits. **(B and C)** Decreased bone remodeling markers of serum Ca^{2+} and serum

alkaline phosphatase (ALP) in the *Prss53*$^{-/-}$ rabbits. **(D)** H&E and immunohistochemistry staining showed the high expression of *Prss53* in the osteoblasts, although not in the *Prss53*$^{-/-}$ rabbits. A significantly reduced number of osteoblasts was determined in the *Prss53*$^{-/-}$ rabbits by H&E staining. **(E)** Statistical analysis showing PRSS53 expression in the osteoblasts, although not in the *Prss53*$^{-/-}$ rabbits. **(F)** Statistical analysis showing a significantly reduced number of osteoblasts in the *Prss53*$^{-/-}$ rabbits. Red arrow indicates the expression of PRSS53 protein in the osteoblasts of WT rabbits. Green arrow indicates the location of osteoblasts in WT rabbits.

Table 1: The expression of calcium metabolism gene

Figure. S1. Generation of *Prss53*$^{-/-}$ rabbits via the CRISPR/Cas9 system

(A) Photographs showing the curved hair of *Prss53*$^{-/-}$ rabbits. **(B)** Agarose gel electrophoresis for mutation detection in F0 generation pups. M: DL2000. Sanger sequencing of the *Prss53* mutant rabbits. The sgRNA sequences are highlighted in red, and PAM sequences are indicated in green. Deletion, "–".

Figure. S2. Off target determination of the *Prss53* mutant rabbits

T7E1 cleavage analysis of POTS for sgRNA1 and sgRNA2. M, DL2000; OT11-15 and OT21-25 represent the ten POTS. The chromatogram sequence analysis of ten POTS for sgRNA and sgRNA2 using PCR products in founder rabbits. The 20 bp of the POTS and PAM are represented in the shaded area.

Figure. S3. Heritability of the *Prss53* mutant rabbits

(A) A male chimera rabbit was mated with female WT rabbits, and there was no hair curvature phenotype in the F1 heterozygous (*Prss53*$^{+/-}$) rabbits. **(B)** The heterozygous (*Prss53*$^{+/-}$) rabbits were mated and used for the generation of homozygous (*Prss53*$^{-/-}$) rabbits. **(C)** Agarose gel electrophoresis for mutation detection of the F1 *Prss53* mutant rabbits. The sgRNA sequences are highlighted in red, and PAM sequences are

indicated in green. Deletion, "–". **(D)** Agarose gel electrophoresis for mutation detection of the F2 *Prss53* mutant rabbits. The sgRNA sequences are highlighted in red, and PAM sequences are indicated in green. Deletion, "–".

Table S1: Primers used for qRT-PCR

Table S2: Primers used for off target

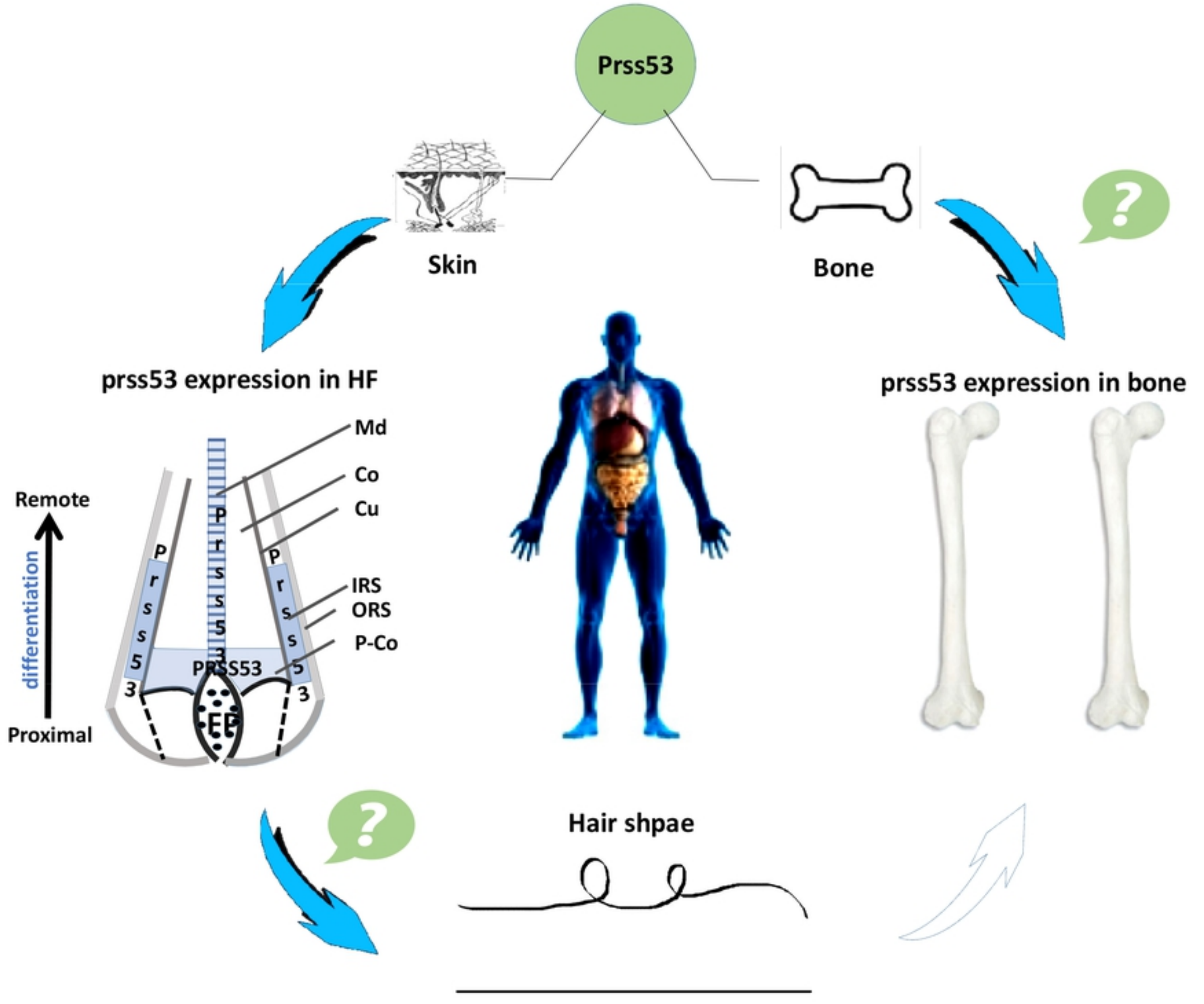

FIG.1

A

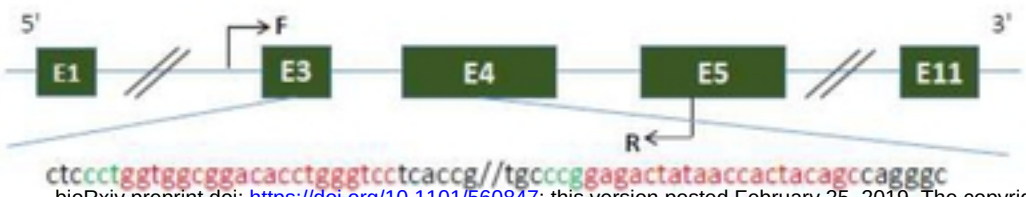

Target gene	Target site	PAM	Oligonucleotide1	Oligonucleotide2
Prss53-sgRNA1	ggacccaggtgtccgccacc	AGG	TAGGACCCAGGTGTCCGCCACC	AAACGGTGGCGGACACCTGGGT
Prss53-sgRNA2	gctgtagtggttatagtctc	CGG	TAGGCTGTAGTGGTTATAGTCTC	AAACGAGACTATAACCACTACAG

B

C

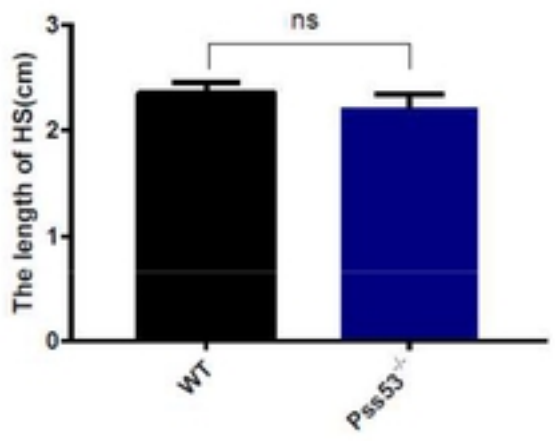

D

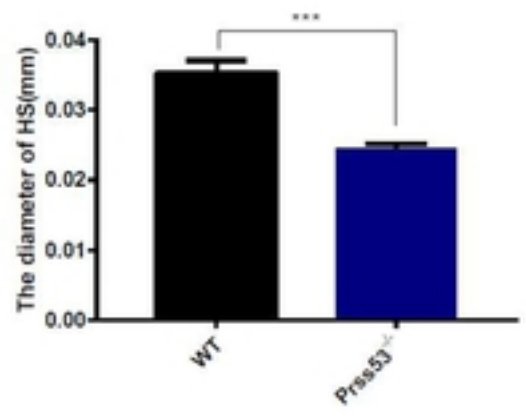

E

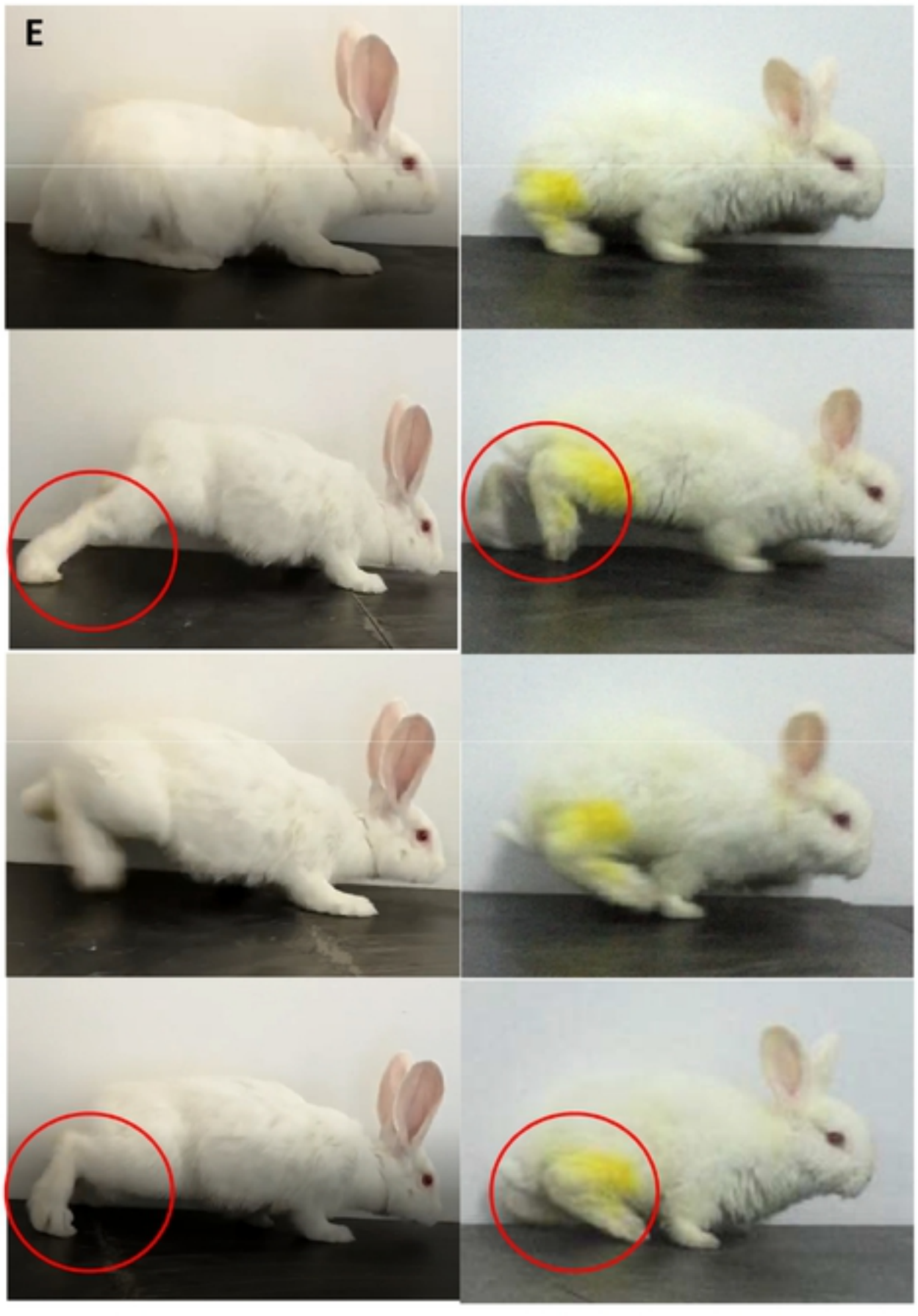

F

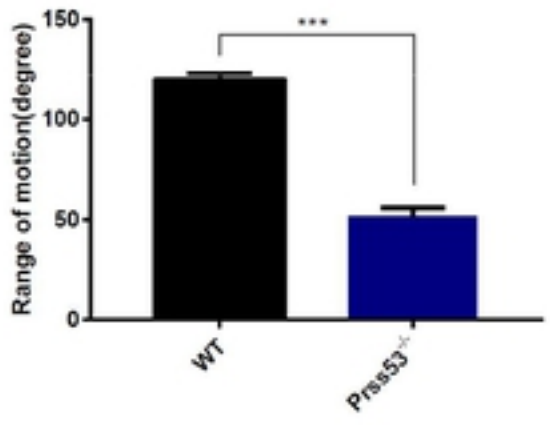

G

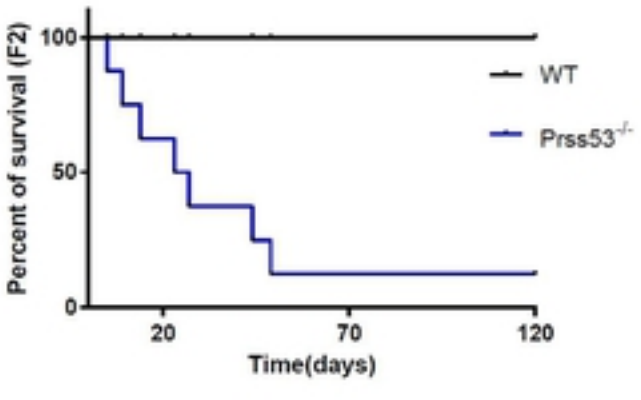

FIG.2

FIG.3

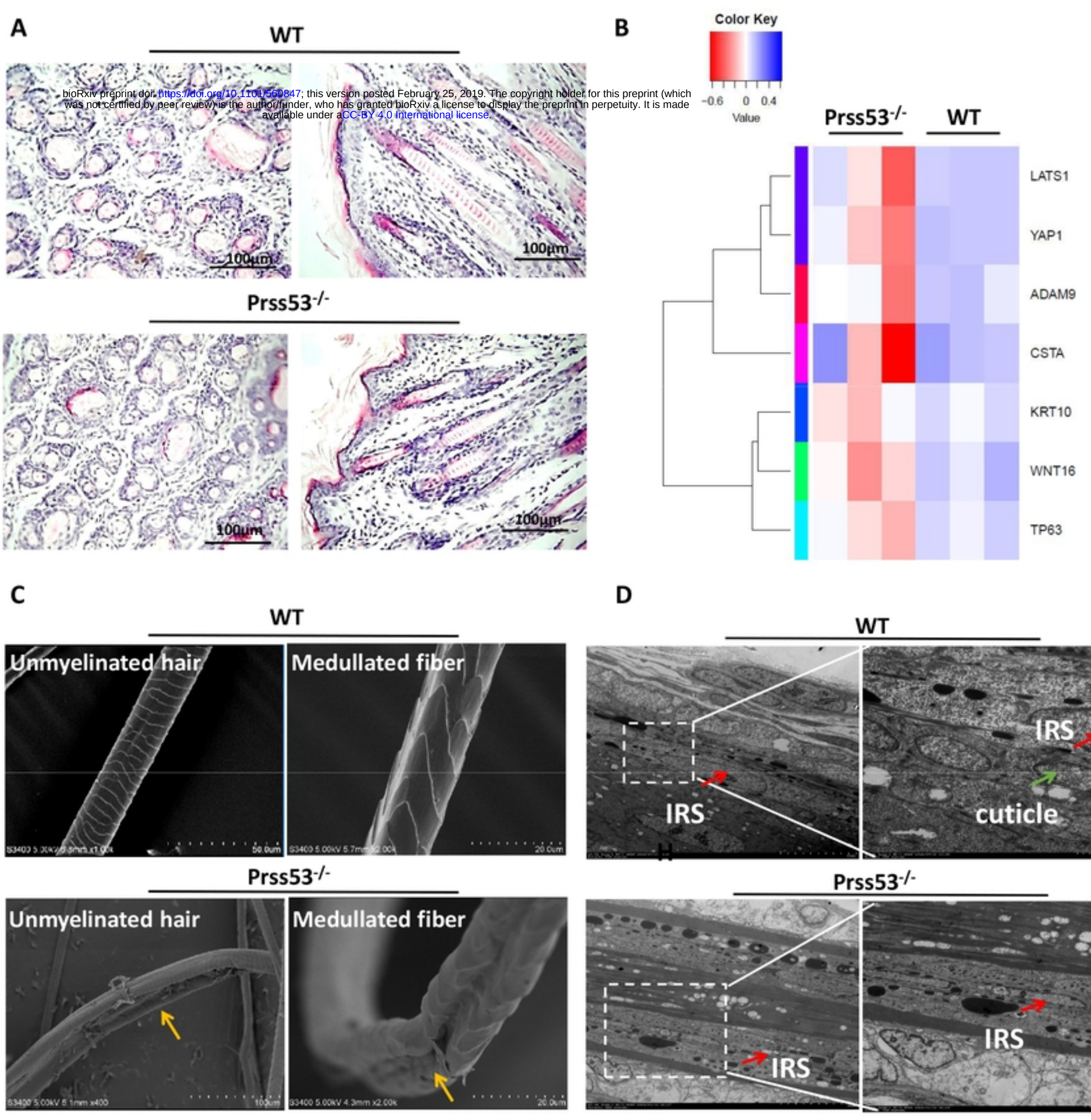

FIG.4

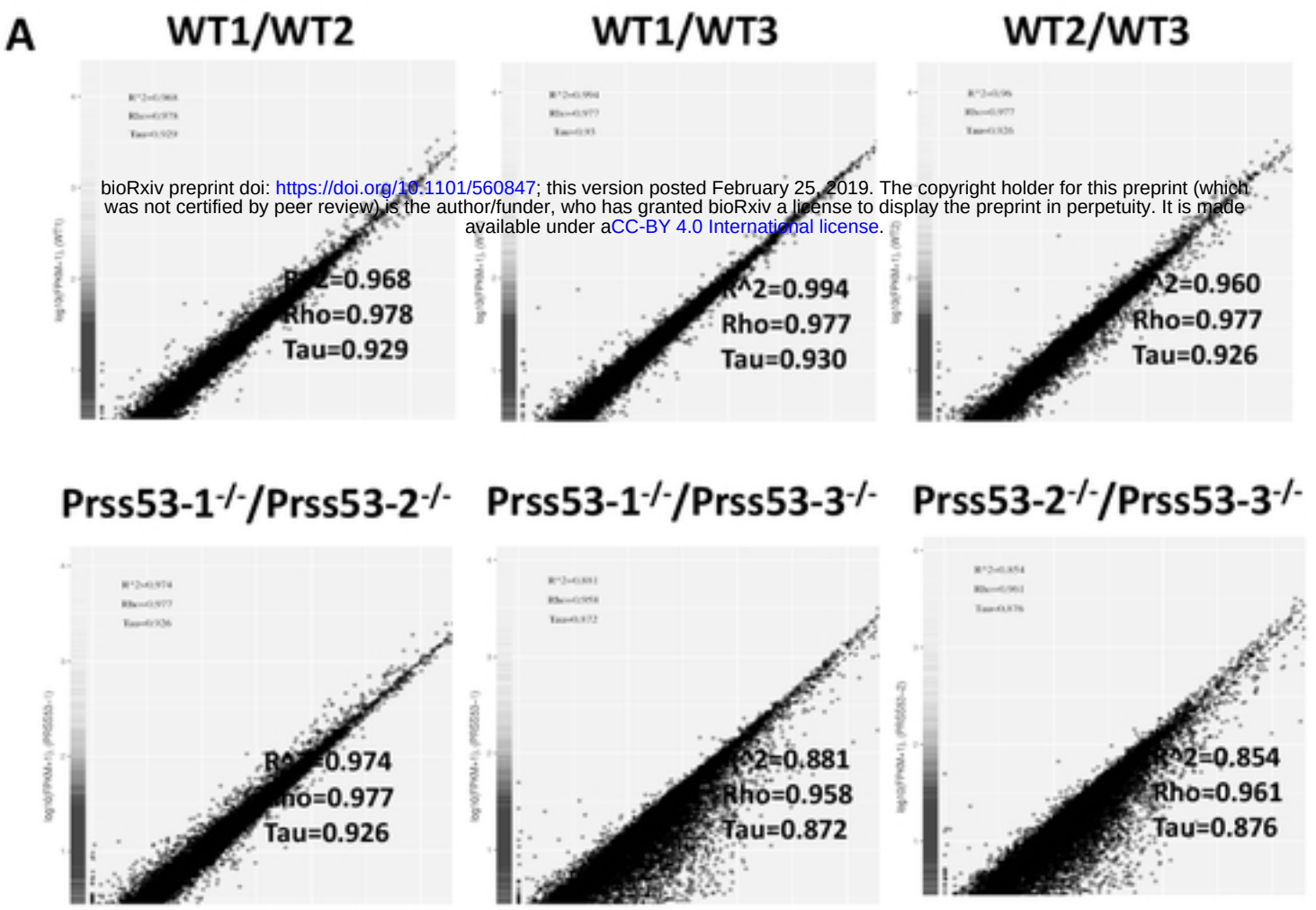

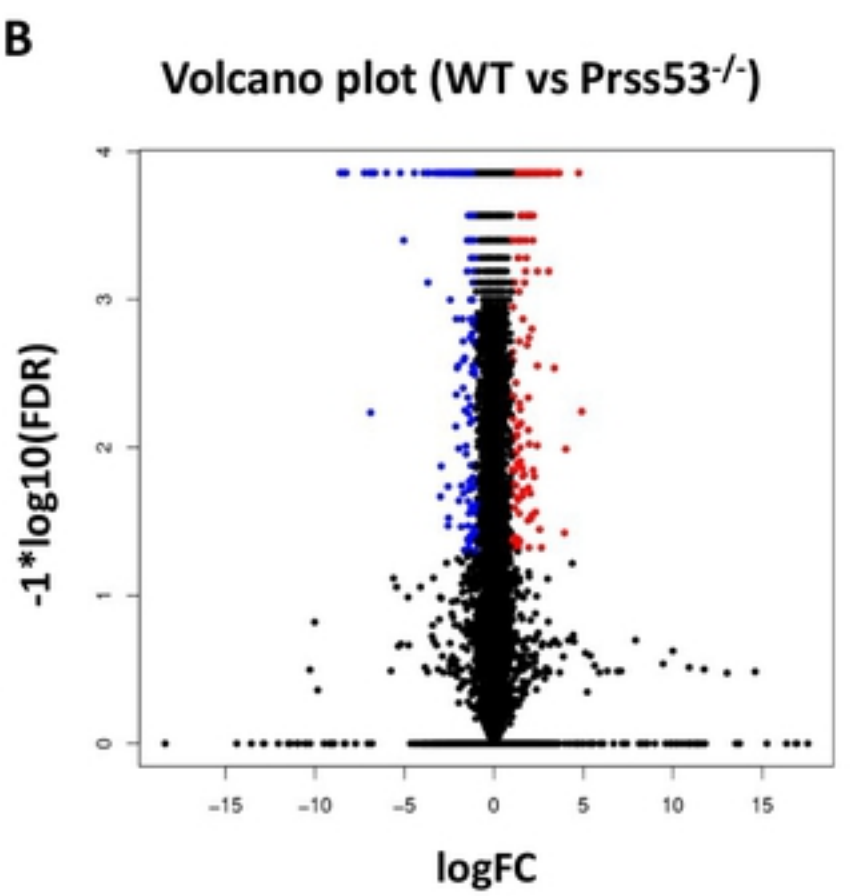

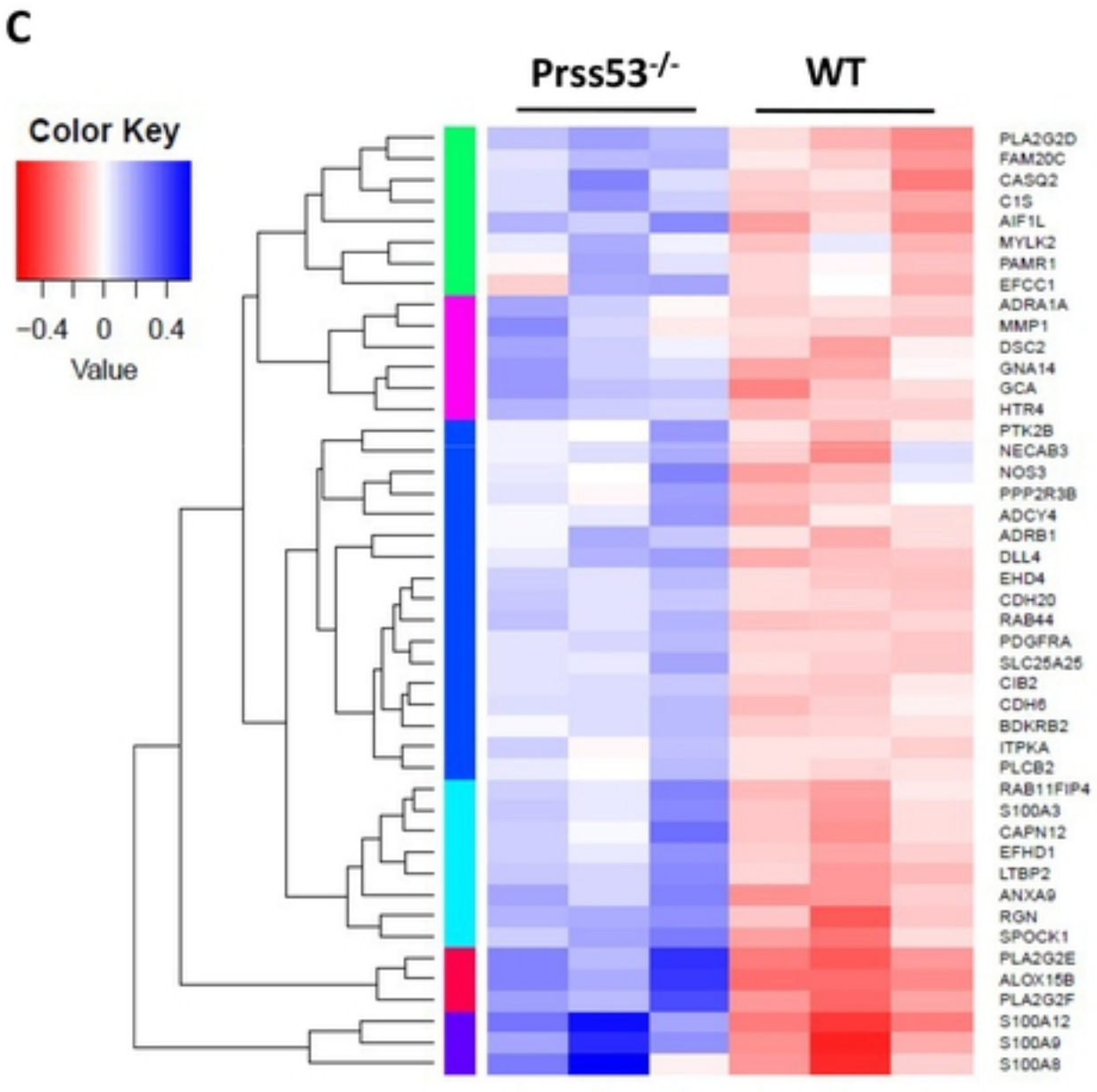

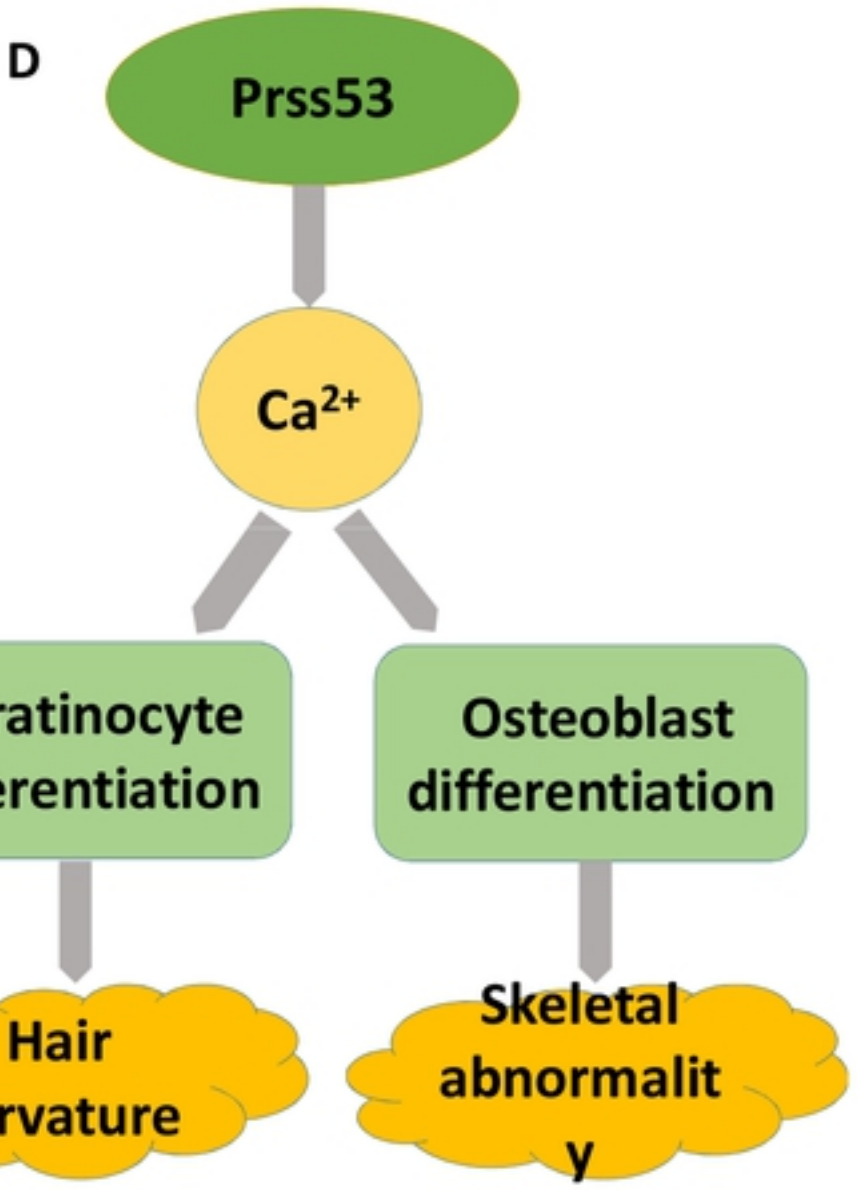

FIG.5

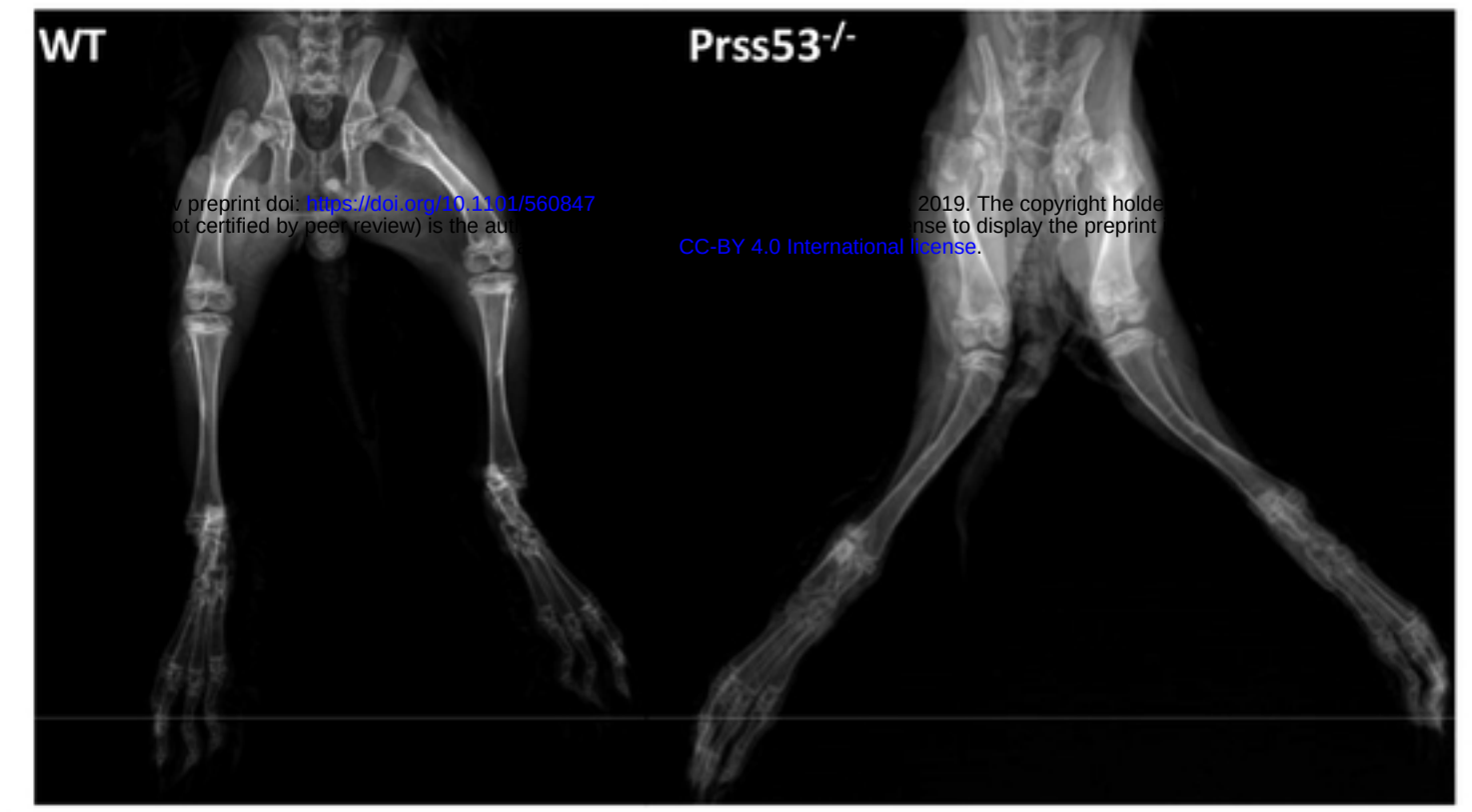

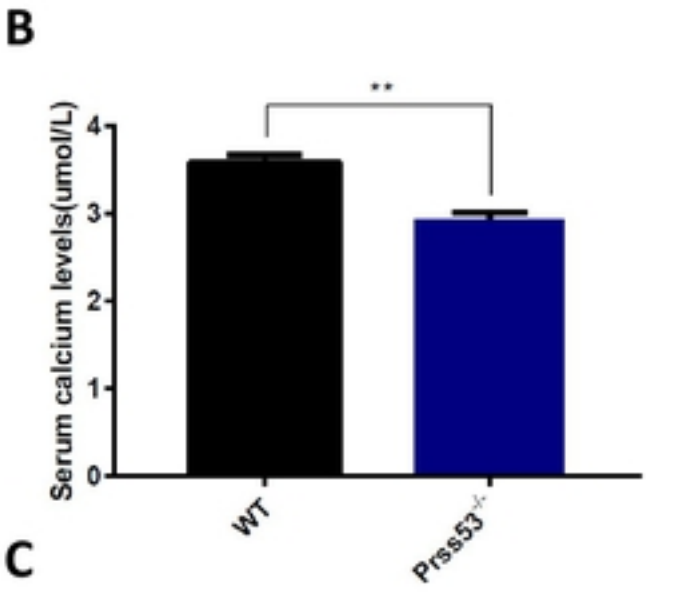

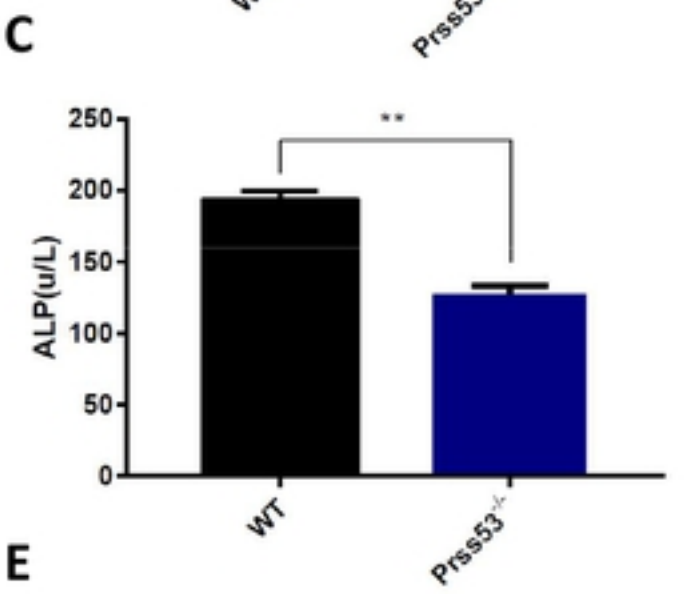

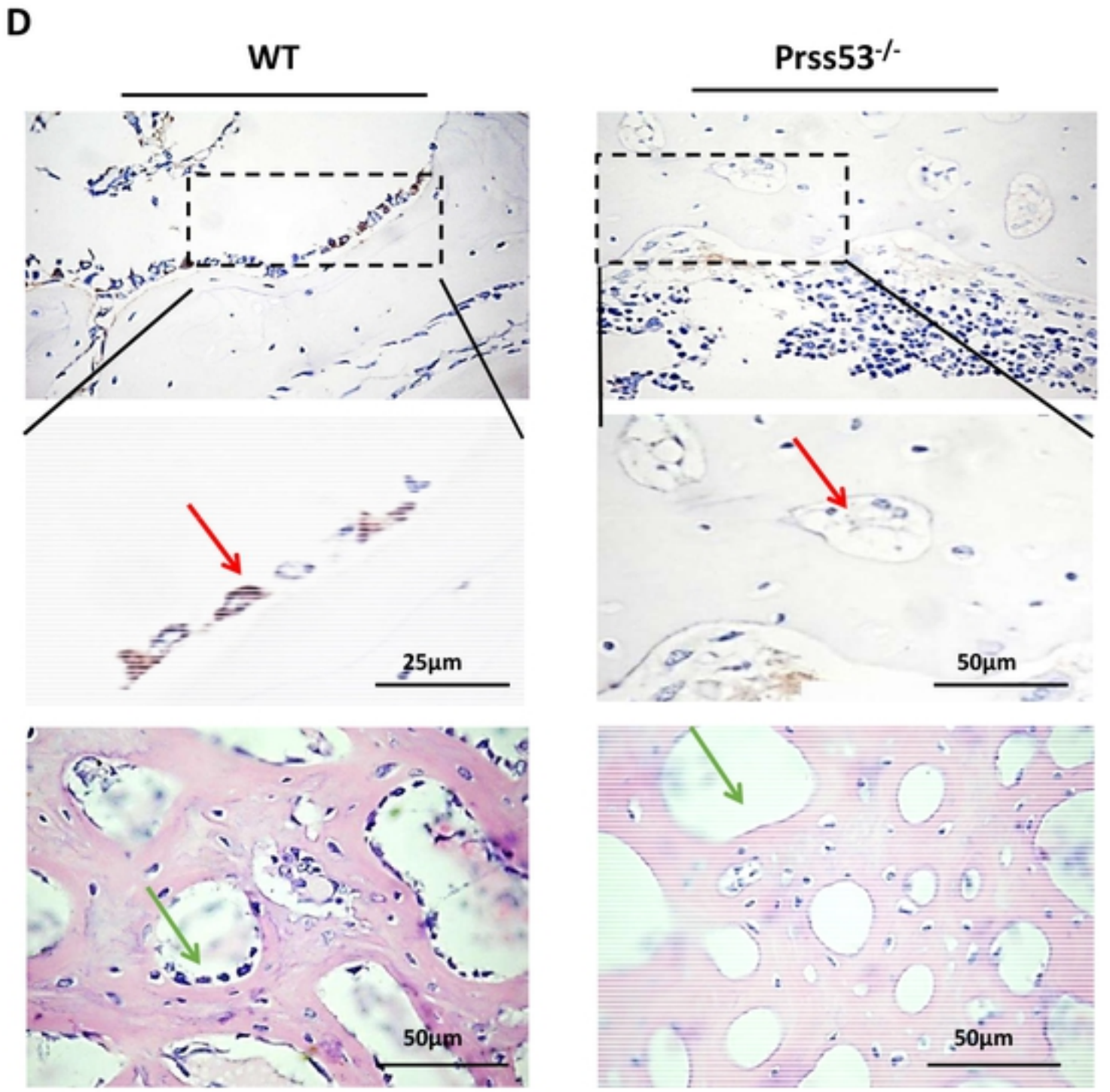

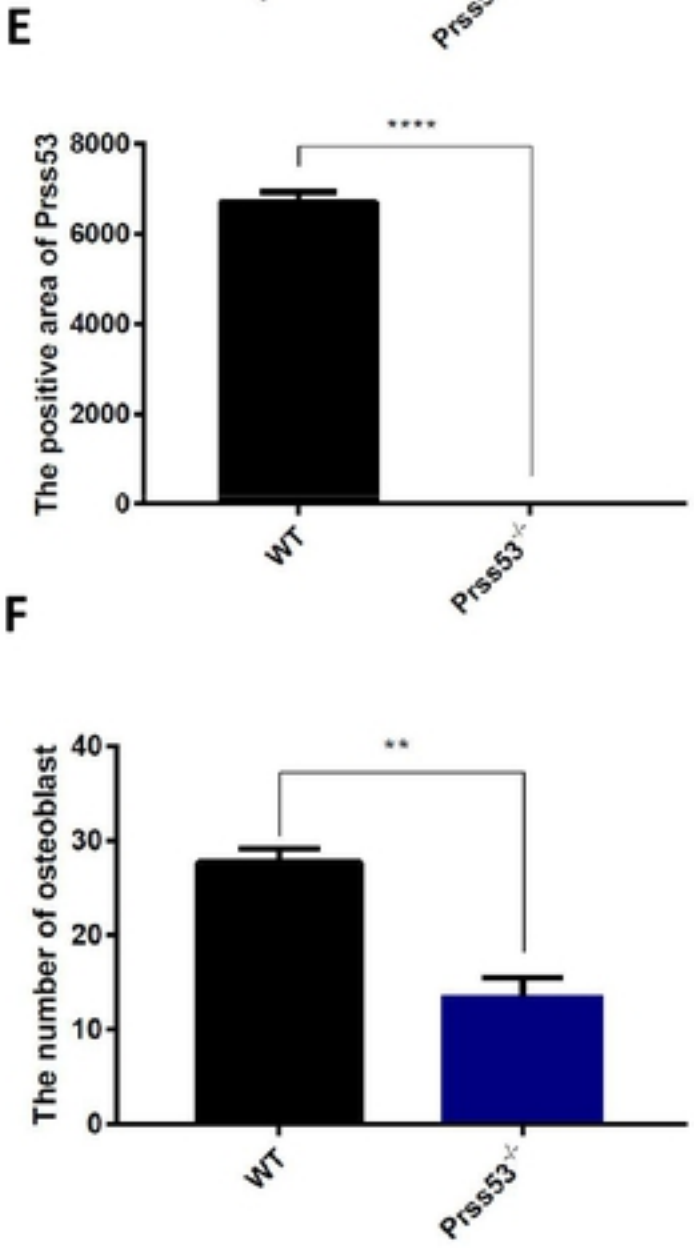

FIG.6

Table 1: The expression of calcium metabolism gene

Gene/probe	Gene accession	Gene name	Fold-change
PLA2G2D	ENSOCUG00000011594	phospholipase A2 group IID	4.38394
FAM20C	ENSOCUG00000010891	FAM20C%2C golgi associated secretory pathway kinase	4.48137
CASQ2	ENSOCUG00000009394	calsequestrin 2	10.5736
C1S	ENSOCUG00000014468	complement C1s	18.1069
AIF1L	ENSOCUG00000024109	allograft inflammatory factor 1 like	4.81457
MYLK2	ENSOCUG00000017328	myosin light chain kinase 2	1.72667
PAMR1	ENSOCUG00000000721	peptidase domain containing associated with muscle regeneration 1	4.03564
EFCC1	ENSOCUG00000022659	EF-hand and coiled-coil domain containing 1	2.03654
ADRA1A	ENSOCUG00000000775	alpha-1A adrenergic receptor	2.24748
MMP1	ENSOCUG00000017958	matrix metallopeptidase 1	3.02895
DSC2	ENSOCUG00000012518	desmocollin 2	15.11
GNA14	ENSOCUG00000005507	G protein subunit alpha 14	3.21548
GCA	ENSOCUG00000002868	grancalcin	3.05625
HTR4	ENSOCUG00000017309	5-hydroxytryptamine receptor 4	4.90416
PTK2B	ENSOCUG00000007668	protein tyrosine kinase 2 beta	6.86819
NECAB3	ENSOCUG00000000850	N-terminal EF-hand calcium binding protein 3	1.49855
NOS3	ENSOCUG00000023757	nitric oxide synthase 3	2.70783
PPP2R3B	ENSOCUG00000000307	protein phosphatase 2 regulatory subunit B''beta	3.683
ADCY4	ENSOCUG00000002958	adenylate cyclase 4	4.18938
ADRB1	ENSOCUG00000007270	adrenoceptor beta 1	0.0166
DLL4	ENSOCUG00000010756	delta like canonical Notch ligand 4	5.6862
EHD4	ENSOCUG00000015759	EH domain containing 4	6.37126
CDH20	ENSOCUG00000014561	cadherin 20	3.67813
RAB44	ENSOCUG00000016053	RAB44%2C member RAS oncogene	3.14484
PDGFRA	ENSOCUG00000000258	platelet derived growth factor receptor alpha	15.3933
SLC25A25	ENSOCUG00000007130	solute carrier family 25 member 25	1.89329
CIB2	ENSOCUG00000016763	calcium and integrin binding family member 2	4.26214
CDH6	ENSOCUG00000000360	cadherin 6	7.32425
BDKRB2	ENSOCUG00000014828	bradykinin receptor B2	2.19751
ITPKA	ENSOCUG00000023580	inositol-trisphosphate 3-kinase A	1.94413
PLCB2	ENSOCUG00000006540	phospholipase C beta 2	2.85937
RAB11FIP4	ENSOCUG00000007443	RAB11 family interacting protein 4	6.75622
S100A3	ENSOCUG00000008647	S100 calcium binding protein A3	32.0311
CAPN12	ENSOCUG00000023100	calpain 12	6.97293
EFHD1	ENSOCUG00000014497	EF-hand domain family member D1	13.6972
LTBP2	ENSOCUG00000014077	latent transforming growth factor beta binding protein 2	16.171
ANXA9	ENSOCUG00000014955	annexin A9	6.72594
RGN	ENSOCUG00000023725	regucalcin	6.20389
SPOCK1	ENSOCUG00000009843	SPARC/osteonectin%2C cwcv and kazal like domains proteoglycan 1	6.04226
PLA2G2E	ENSOCUG00000006574	phospholipase A2 group IIE	20.4203
ALOX15B	ENSOCUG00000010340	arachidonate 15-lipoxygenase%2C type B	9.99443
PLA2G2F	ENSOCUG00000004126	phospholipase A2 group IIF	22.4474
S100A12	ENSOCUG00000022646	S100 calcium binding protein A12	22.4474
S100A9	ENSOCUG00000008632	S100 calcium binding protein A9	9.03642
S100A8	ENSOCUG00000009566	S100 calcium binding protein A8	5.08249

Table.1